Pseudo-Stereo for Monocular 3D Object Detection in Autonomous Driving
Supplementary Material

Yi-Nan Chen[1] Hang Dai[2*] Yong Ding[1*]
[1]School of Micro-Nano Electronics, Zhejiang University
[2]Mohamed bin Zayed University of Artificial Intelligence, Abu Dhabi, UAE
[*]Corresponding authors{hang.dai@mbzuai.ac.ae, dingy@vlsi.zju.edu.cn}.

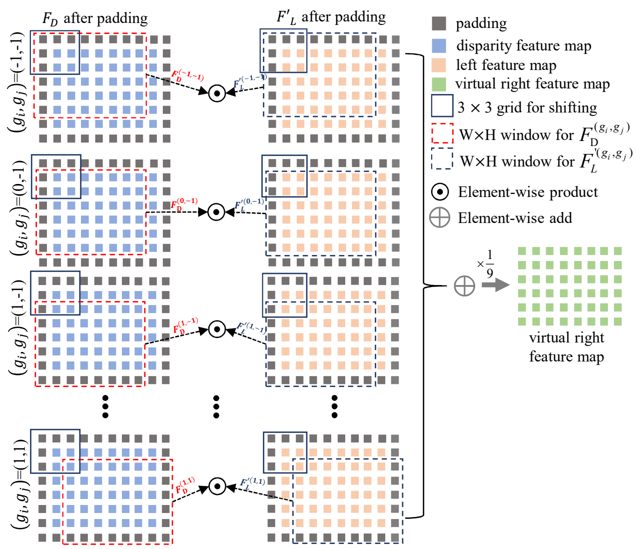

Figure 1. An illustration of disparity-wise dynamic convolution with grid shifting. The top left corner point of W $\times$ H window (blue and red dot windows for disparity feature map and left feature map, respectively) shifts within the 3×3 grid (blue box). The outcome (virtual right feature map) of the overall operation with 9 times W $\times$ H window shifting in 3×3 grid is the same as that of the overall operation with W $\times$ H times 3×3 sliding window to cover the whole feature map.

1. Disparity-wise Dynamic Convolution with Grid Shifting

The process of disparity-wise dynamic convolution with grid shifting can formulated as:

$$\hat{F}'_R = \frac{1}{3\times 3}\sum_{g_i,g_j} F_L'^{(g_i,g_j)} \odot F_D^{(g_i,g_j)} \tag{1}$$

where $\hat{F}'_R$ is the generated virtual right feature map, F'_L indicates the left feature map and F_D is the disparity feature map. The (g_i, g_j) indicates the shifting direction and step size within the 3×3 grid $\{(g_i, g_j)\}$, where $g \in \{-1, 0, 1\}$.

Also, the Eqn. 1 can be expanded as follows:

$$\begin{aligned}\hat{F}'_R = \frac{1}{3\times 3}(&F_L'^{(-1,-1)} \odot F_D^{(-1,-1)} \\ &+ F_L'^{(-1,0)} \odot F_D^{(-1,0)} + F_L'^{(-1,1)} \odot F_D^{(-1,1)} \\ &+ F_L'^{(0,-1)} \odot F_D^{(0,-1)} + F_L'^{(0,0)} \odot F_D^{(0,0)} \\ &+ F_L'^{(0,1)} \odot F_D^{(0,1)} + F_L'^{(1,-1)} \odot F_D^{(1,-1)} \\ &+ F_L'^{(1,0)} \odot F_D^{(1,0)} + F_L'^{(1,1)} \odot F_D^{(1,1)})\end{aligned} \tag{2}$$

We illustrate the above process in Figure 1. The top left corner point of W $\times$ H window (blue and red dot windows for disparity feature map and left feature map, respectively) shifts within the 3×3 grid (blue box). The outcome (virtual right feature map) of the overall operation with 9 times W $\times$ H window shifting in 3×3 grid is the same as that of the overall operation with W $\times$ H times 3×3 sliding window to cover the whole feature map.

2. Right Feature Re-projection in Feature-clone

In the main paper, we follow LIGA-stereo [3] to concatenate the left features F_L and the re-projected right features $F_{R->L}$ at all candidate depth levels for building the stereo volume V_{st} as follows:

$$V_{st}(u, v, w) = concat[F_L(u, v), F_{R->L}(u, v)] \tag{3}$$

$$F_{R->L}(u, v) = F_R(u - \frac{f\cdot b}{d(w)\cdot S}, v) \tag{4}$$

$$d(w) = w \cdot v_d + z_{min} \tag{5}$$

where (u, v) are the pixel coordinates, $w \in [0, 1, ...]$ indicates the depth index, S is the stride of the feature map, v_d is the depth interval, z_{min} indicates the minimal depth value, f is the camera focal length, and b represents the baseline of the stereo camera pair. In feature-clone virtual right view generation method, we duplicate the left features F_L as the right features $\hat{F}_R$ and concatenate the left features F_L and re-projected right features $F_{R->L}$ as described in Eqn. 3.

Methods	AP_{3D}/AP_{BEV} Easy	Moderate	Hard
Ours-fcd w/ re-projection	**28.46 / 37.66**	**19.15 / 25.78**	**16.56 / 22.47**
Ours-fcd w/o re-projection	22.36/ 31.49	16.19 / 22.68	14.19/ 20.48

Table 1. Performance for *Car* on KITTI *val* set at IOU threshold 0.7. Compare the performance with and without re-projection. We report the results in $AP|_{R40}$.

To show the effectiveness of the right feature re-projection, we conduct an experiment using the the concatenation of the left features F_L and the virtual right features $\hat{F}_R$ without re-projection as:

$$V^*_{st}(u, v, w) = concat[F_L(u, v), \hat{F}_R(u, v)] \tag{6}$$

As shown in Table. 1, without re-projection, the performance of the proposed framework decreases significantly in AP_{3D} by (-6.1%, -2.96%, -2.37%) and AP_{BEV} by (-6.17%, -3.1%, -1.99%). This implies that the re-projection of right feature is effective in constructing the stereo volume for monocular 3D detection.

Exp.	Methods	L_{depth}	L_{kd}	AP_{3D}/AP_{BEV} Easy	Moderate	Hard
1	Image-level	✓	✓	31.43 / 41.82	21.53 / 29.00	18.47 / 25.21
2	Image-level		✓	**31.81 / 42.87**	**22.36 / 30.16**	**19.33 / 26.38**
3	Image-level	✓		29.10 / 39.61	20.12 / 27.60	17.07 / 23.16
4	Image-level			28.89 / 40.17	20.79 / 29.45	17.81 / 25.14
5	Feature-level	✓	✓	**35.18 / 45.50**	**24.15 / 32.03**	**20.35 / 27.57**
6	Feature-level		✓	22.04 / 31.10	16.18 / 22.55	14.31 / 20.56
7	Feature-level	✓		32.48 / 43.62	22.38 / 30.78	19.23 / 26.94
8	Feature-level			19.37 / 29.44	14.10 / 21.26	12.55 / 19.22
9	Feature-clone	✓	✓	**28.46 / 37.66**	**19.15 / 25.78**	**16.56 / 22.47**
10	Feature-clone		✓	24.33 / 32.99	17.09 / 23.77	14.61 / 20.81
11	Feature-clone	✓		24.20 / 33.69	17.02 / 23.85	14.73 / 21.26
12	Feature-clone			19.69 / 28.96	14.56 / 21.32	12.94 / 19.04

Table 2. Ablation studies of three proposed Pseudo-Stereo variants, L_{depth} and L_{kd} at IOU threshold 0.7. Exp. is the experiment tag. We report the results in $AP|_{R40}$.

3. The Effect of Knowledge Distillation

Although LIGA-stereo has studied the effect of knowledge distillation in [3], we conduct an extra study of knowledge distillation for the proposed Pseudo-Stereo frameworks in supplementary material as shown in Table. 2. The proposed frameworks without the knowledge distillation still achieve decent performance on KITTI *val* set. As discussed and analyzed in the main paper, the depth loss is not effective for image-level generation. Knowledge distillation improves the detection performance, which is consistent with the study in LIGA-stereo [3]. This lies in the fact that knowledge distillation transfers the structural detection knowledge from LiDAR-based 3D detectors. Note that we focus on the analysis of depth-aware feature learning in the main paper and discuss the knowledge distillation that is not related to depth-aware feature learning in supplementary material.

Methods	L_{disp}	AP_{3D}/AP_{BEV} Easy	Moderate	Hard
Pseudo-LiDAR [8]	–	– / 28.20	– / 18.50	– / 16.40
AM3D [6]	–	– / <u>32.23</u>	– / 21.09	– / 17.26
DDMP-3D [7]	–	<u>28.12</u> / 31.14	<u>20.39</u> / <u>23.12</u>	**16.34** / <u>19.45</u>
M3D-RPN [1]	–	14.53 / 20.27	11.07 / 17.06	8.65 / 15.21
D4LCN [2]	–	22.32 / 26.97	16.20 / 21.71	12.30 / 18.22
YOLOMono3D [5]	–	21.66 / –	14.20 / –	11.07 / –
Ours + YOLOStereo3D [5]	✓	**33.74 / 44.95**	**21.56 / 28.04**	<u>15.58</u> / **21.87**
Ours + YOLOStereo3D [5]		17.79 / 28.01	11.20 / 17.63	8.81 / 13.55

Table 3. Performance for *Car* on KITTI *val* set at IOU threshold 0.7. L_{disp} indicates disparity loss. The best results are **bold**, and the second best results are <u>underlined</u>. We report the results in $AP|_{R40}$.

4. YOLOStereo3D with Pseudo-Stereo Views

We apply the feature-level virtual view generation that is our best method to the stereo 3D detector YOLOStereo3D [5] for monocular 3D detection. Note that the YOLO is a general architecture for image-based detection tasks, and our method is effective with a general image-based detection architecture for detecting 3D objects from a single image.

Preliminaries of YOLOStereo3D. The network architecture of YOLOStereo3D [5] includes four components. **(I)** A ResNet-34 [4] with shared weights is used to extract the multi-scale features from the left-right image pair. **(II)** A multi-scale stereo matching and fusion module is used to fuse the left features and the right features. **(III)** Disparity estimation head, and **(IV)** 3D detection head.

Implementation Details. We only modify the component **I** and use our feature-level generation method to generate the multi-scale virtual right features to adapt YOLOStereo3D to monocular 3D detection. For training, the batch size is set to 8 and other hyper-parameters are set the same as YOLOStereo3D [5]. To show the effect of the disparity loss, we conduct two experiments with disparity loss and without disparity loss.

Results. As shown in Table. 3, The adaptation of YOLOStereo3D [5] to monocular 3D detection with our Pseudo-Stereo views achieves significant improvements against YOLOMono3D [5] that is the official monocular version of YOLOStereo3D [5]. Also, it achieves better performance in monocular 3D detection than other state-of-the-art monocular 3D detectors, such as Pseudo-LiDAR [8], AM3D [6], DDMP-3D [7], M3D-RPN [1] and D4LCN [2]. With the disparity loss that is originally assembled in YOLOStereo3D [5], the adaptation of YOLOStereo3D [5] to monocular 3D detection with our Pseudo-Stereo views achieves significant improvements, which lies in the depth-aware feature learning with the disparity guidance in the

Input	Output	Module Config	Channel	Size
$I_L, \hat{I}_R$	$conv1$	7 × 7 Conv, stride=2	64	$H/2 \times W/2$
$conv1$	$conv2$	BasicBlock × 3, dilation=1, stride=1	64	$H/2 \times W/2$
$conv2$	$conv3$	BasicBlock × 4, dilation=1, stride=2	128	$H/4 \times W/4$
$conv3$	$conv4$	BasicBlock × 6, dilation=2, stride=1	128	$H/4 \times W/4$
$conv4$	$conv5$	BasicBlock × 3, dilation=4, stride=1	128	$H/4 \times W/4$
$conv5$	$spp1$	AvgPool (64×64);1×1 Conv; Upsample 64×	32	$H/4 \times W/4$
$conv5$	$spp2$	AvgPool (32×32);1×1 Conv; Upsample 32×	32	$H/4 \times W/4$
$conv5$	$spp3$	AvgPool (16×16);1×1 Conv; Upsample 16×	32	$H/4 \times W/4$
$conv5$	$spp4$	AvgPool (8×8);1×1 Conv; Upsample 8×	32	$H/4 \times W/4$
spp1-4, $conv$3-5	spp	Concat	512	$H/4 \times W/4$
$conv2$	$hres1$	1×1 Conv	64	$H/2 \times W/2$
$I_L, \hat{I}_R$	$hres2$	1×1 Conv	32	$H \times W$
spp	$up1$	3×3 Conv; Upsample 2×; Add $hres1$; ReLU	64	$H/2 \times W/2$
$up1$	$up2$	3×3 Conv; Upsample 2×; Add $hres2$; ReLU	32	$H \times W$
$up2$	$F_{L/R}$	3×3 Conv × 2	32, 32	$H \times W$
$F_{L/R}$	V_{st}	Build stereo volume(Eqn. 3), disparity downsample=1	64	$D/4 \times H/4 \times W/4$

Table 4. Architecture details of stereo image feature extraction with *image-level generation*.

Input	Output	Module Config	Channel	Size
I_L, D	$conv1$	7 × 7 Conv, stride=2	64	$H/2 \times W/2$
$conv1$	$conv2$	BasicBlock × 3, dilation=1, stride=1	64	$H/2 \times W/2$
$conv2$	$conv3$	BasicBlock × 4, dilation=1, stride=2	128	$H/4 \times W/4$
$conv3$	$conv4$	BasicBlock × 6, dilation=2, stride=1	128	$H/4 \times W/4$
$conv4$	$conv5$	BasicBlock × 3, dilation=4, stride=1	128	$H/4 \times W/4$
$conv3$	$conv3'$	DDC	128	$H/4 \times W/4$
$conv4$	$conv4'$	DDC	128	$H/4 \times W/4$
$conv5$	$conv5'$	DDC	128	$H/4 \times W/4$
$conv5'$	$spp1$	AvgPool (64×64);1×1 Conv; Upsample 64×	32	$H/4 \times W/4$
$conv5'$	$spp2$	AvgPool (32×32);1×1 Conv; Upsample 32×	32	$H/4 \times W/4$
$conv5'$	$spp3$	AvgPool (16×16);1×1 Conv; Upsample 16×	32	$H/4 \times W/4$
$conv5'$	$spp4$	AvgPool (8×8);1×1 Conv; Upsample 8×	32	$H/4 \times W/4$
spp1-4, $conv3'$-$5'$	spp	Concat	512	$H/4 \times W/4$
spp	$F_{L/R}$	3×3 Conv × 2	32, 32	$H/4 \times W/4$
$F_{L/R}$	V_{st}	Build stereo volume(Eqn. 3), disparity downsample=4	64	$D/4 \times H/4 \times W/4$

Table 5. Architecture details of stereo image feature extraction with *feature-level generation*.

Input	Output	Module Config	Channel	Size
I_L	$conv1$	7 × 7 Conv, stride=2	64	$H/2 \times W/2$
$conv1$	$conv2$	BasicBlock × 3, dilation=1, stride=1	64	$H/2 \times W/2$
$conv2$	$conv3$	BasicBlock × 4, dilation=1, stride=2	128	$H/4 \times W/4$
$conv3$	$conv4$	BasicBlock × 6, dilation=2, stride=1	128	$H/4 \times W/4$
$conv4$	$conv5$	BasicBlock × 3, dilation=4, stride=1	128	$H/4 \times W/4$
$conv5$	$spp1$	AvgPool (64×64);1×1 Conv; Upsample 64×	32	$H/4 \times W/4$
$conv5$	$spp2$	AvgPool (32×32);1×1 Conv; Upsample 32×	32	$H/4 \times W/4$
$conv5$	$spp3$	AvgPool (16×16);1×1 Conv; Upsample 16×	32	$H/4 \times W/4$
$conv5$	$spp4$	AvgPool (8×8);1×1 Conv; Upsample 8×	32	$H/4 \times W/4$
spp1-4, $conv$3-5	spp	Concat	512	$H/4 \times W/4$
spp	$F_{L/R}$	3×3 Conv × 2; Clone	32, 32	$H/4 \times W/4$
$F_{L/R}$	V_{st}	Build stereo volume(Eqn. 3), disparity downsample=4	64	$D/4 \times H/4 \times W/4$

Table 6. Architecture details of stereo image feature extraction with *feature clone*.

overall loss function.

5. The architecture details of the proposed three methods

In the paper, we propose three novel methods to generate the virtual right view: (a) *image-level generation*, (b) *feature-level generation* and (c) *feature-clone*. We use LIGA-Stereo [3] as our base stereo 3D architecture and feed the Pseudo-Stereo views to LIGA-Stereo. We only modify the component of stereo image feature extraction in LIGA-Stereo [3] for monocular 3D detection. Table. 4 shows the architecture of stereo image feature extraction with *image-level generation*. Table. 5 shows the architecture of stereo image feature extraction with *feature-level generation*. Table. 6 the architecture of stereo image feature extraction with *feature-clone*.

References

[1] Garrick Brazil and Xiaoming Liu. M3d-rpn: Monocular 3d region proposal network for object detection. In *Proceedings of the IEEE International Conference on Computer Vision*, pages 9287–9296, 2019.

[2] Mingyu Ding, Yuqi Huo, Hongwei Yi, Zhe Wang, Jianping Shi, Zhiwu Lu, and Ping Luo. Learning depth-guided convolutions for monocular 3d object detection. *arXiv preprint arXiv:1912.04799*, 2019.

[3] Xiaoyang Guo, Shaoshuai Shi, Xiaogang Wang, and Hongsheng Li. Liga-stereo: Learning lidar geometry aware representations for stereo-based 3d detector. In *Proceedings of the IEEE/CVF International Conference on Computer Vision*, pages 3153–3163, 2021.

[4] Kaiming He, Xiangyu Zhang, Shaoqing Ren, and Jian Sun. Deep residual learning for image recognition. In *Proceedings of the IEEE conference on computer vision and pattern recognition*, pages 770–778, 2016.

[5] Yuxuan Liu, Lujia Wang, and Ming Liu. Yolostereo3d: A step back to 2d for efficient stereo 3d detection. *arXiv preprint arXiv:2103.09422*, 2021.

[6] Xinzhu Ma, Zhihui Wang, Haojie Li, Pengbo Zhang, Wanli Ouyang, and Xin Fan. Accurate monocular 3d object detection via color-embedded 3d reconstruction for autonomous driving. In *Proceedings of the IEEE International Conference on Computer Vision*, pages 6851–6860, 2019.

[7] Li Wang, Liang Du, Xiaoqing Ye, Yanwei Fu, Guodong Guo, Xiangyang Xue, Jianfeng Feng, and Li Zhang. Depth-conditioned dynamic message propagation for monocular 3d object detection. In *Proceedings of the IEEE/CVF Conference on Computer Vision and Pattern Recognition*, pages 454–463, 2021.

[8] Yan Wang, Wei-Lun Chao, Divyansh Garg, Bharath Hariharan, Mark Campbell, and Kilian Q Weinberger. Pseudo-lidar from visual depth estimation: Bridging the gap in 3d object detection for autonomous driving. In *Proceedings of the IEEE Conference on Computer Vision and Pattern Recognition*, pages 8445–8453, 2019.